Excitons in T-shaped quantum wires

M. H. Szymanska,[1] P. B. Littlewood[1,2] and R. J. Needs[1]
[1]*Theory of Condensed Matter, Cavendish Laboratory, Cambridge CB3 0HE, United Kingdom*
[2]*Bell Laboratories, Lucent Technologies, Murray Hill, New Jersey 07974*
(Received 15 November 2000; published 2 May 2001)

We calculate energies, oscillator strengths for radiative recombination, and two-particle wave functions for the ground-state exciton and around 100 excited states in a T-shaped quantum wire. We include the single-particle potential and the Coulomb interaction between the electron and hole on an equal footing, and perform exact diagonalization of the two-particle problem within a finite-basis set. We calculate spectra for all of the experimentally studied cases of T-shaped wires including symmetric and asymmetric $GaAs/Al_xGa_{1-x}As$ and $In_yGa_{1-y}As/Al_xGa_{1-x}As$ structures. We study in detail the shape of the wave functions to gain insight into the nature of the various states for selected symmetric and asymmetric wires in which laser emission has been experimentally observed. We also calculate the binding energy of the ground-state exciton and the confinement energy of the one-dimensional (1D) quantum-wire-exciton state with respect to the 2D quantum-well exciton for a wide range of structures, varying the well width and the Al molar fraction x. We find that the largest binding energy of any wire constructed to date is 16.5 meV. We also notice that in asymmetric structures, the confinement energy is enhanced with respect to the symmetric forms with comparable parameters but the binding energy of the exciton is then lower than in the symmetric structures. For $GaAs/Al_xGa_{1-x}As$ wires we obtain an upper limit for the binding energy of around 25 meV in a 10-Å -wide GaAs/AlAs structure that suggests that other materials must be explored in order to achieve room-temperature applications. There are some indications that $In_yGa_{1-y}As/Al_xGa_{1-x}As$ might be a good candidate.

DOI: 10.1103/PhysRevB.63.205317 PACS number(s): 78.67.Lt, 73.21.Hb

I. INTRODUCTION

Optical properties of electrons and holes confined to few dimensions are of interest for optical and electronic devices. As the dimensionality of the structure is reduced, the density of states tends to bunch together leading to a singularity in the one-dimensional (1D) case. This effect can be very useful for low-threshold laser applications. At the same time the excitonic interaction in 1D is enhanced with respect to that in 3D and 2D structures. Quantum confinement leads to an increase in the exciton binding energy E_b and the oscillator strength for radiative recombination. Both effects provide possibilities for much better performance of optical devices such as semiconductor lasers.

The binding energy of a ground-state exciton in an ideal 2D quantum well is four times that in the 3D bulk semiconductor. For the ideal 1D quantum wire E_b diverges. This suggests that E_b for quasi-1D wires can be greatly increased with respect to the 2D limit for very thin wires with high-potential barriers. 3D and 2D excitons dissociate at room temperature to form an electron-hole plasma. To make them useful for real device applications, their binding energy needs to be increased and this might be achieved by using 1D quantum confinement.

Technologically it is very difficult to manufacture good-quality 1D quantum wires with confinement in both spatial directions. They can be obtained from a 2D quantum well, fabricated by thin-film growth, by lateral structuring using lithographic methods. The accuracy of this method is, however, limited to some 10 nm and thus the electronic properties of samples constructed in this way typically have a strong-inhomogeneous broadening. Fortunately it appears possible to achieve quasi-1D particles even without a rigorous confinement in any of the spatial directions. This has been realized in so-called V- and T-shaped quantum wires. V-shaped quantum wires are obtained by self-organized growth in prepatterned materials such as chemically etched V-shaped grooves in GaAs substrates. The T-shaped quantum wire, first proposed by Chang *et al.*,[1] forms at the intersection of two quantum wells and is obtained by the cleaved-edge over-growth method, a molecular-beam epitaxy technique. The accuracy of this method is extremely high and allows fabrication of very thin (less than the Bohr radius of an exciton) wires with small thickness fluctuations. These structures are currently the subject of intensive research and have been realized by several groups.[2–8]

Experimentalists try to optimize the geometry and the materials in order to increase the binding energy of the excitons E_b and the confinement energy E_{con} for possible room-temperature applications. Until now, the most popular material studied experimentally has been $GaAs/Al_xGa_{1-x}As$. Increasing the Al molar fraction x should lead to bigger E_b and E_{con} but, unfortunately, for larger x the interfaces get rougher that degrades the transport properties. Thus optimized geometries for lower values of x become more relevant.

The confinement energy E_{con} is the energy difference between the lowest excitonic state in the wire and the lowest excitonic state in the 2D quantum well. It can be directly measured as the difference between the photoluminescence peaks obtained in a quantum wire (QWR) and a quantum well (QW). It is, however, not possible to measure the exci-

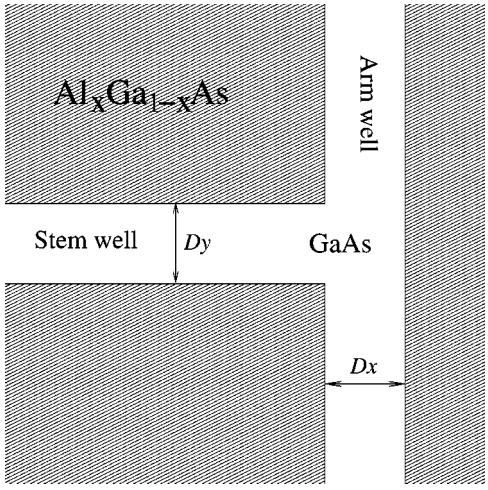

FIG. 1. Shape of the symmetric T-shaped wire with notations.

ton binding energy directly. Its value has to be obtained froma combination of experimental data and one-particle calculations of electron and hole energies in a wire. There has been a disagreement between the purely theoretical values[9–13] and those obtained from a combination of experimental data and theoretical calculations. The confinement energies, however, tend to agree between experiment and purely theoretical calculations, suggesting that experiment, using combined methods where errors tend to accumulate, usually overestimates the binding energy.

For the 5-nm scale symmetric GaAs/AlAs, Someya *et al.*[3] reported the largest confinement energy for excitons in symmetric wires (Fig. 1), $E_{con}=38$ meV and $E_b=27\pm3$ meV. The largest confinement energy of any structure was reported by Gislason and co-workers[4,5] for their optimized wires. Using asymmetric wells with different widths and Al content as in Fig. 2, they obtained an exciton-confinement energy of 54 meV. Recently there has also been the first experimental realization of T-shaped wires using $In_yGa_{1-y}As/Al_{0.3}Ga_{0.7}As$.[2] The highest confinement energy reported for this structure is 34 meV, which is very close to the GaAs/AlAs result, and

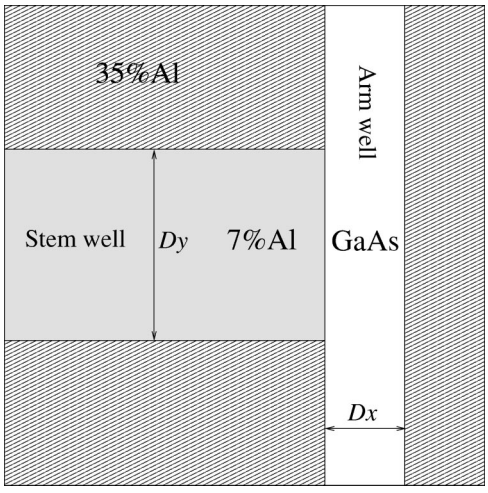

FIG. 2. Shape of the asymmetric T-shaped wire with notations.

the quality of the structure can be much higher than for the GaAs/AlAs case.

Laser emission from the lowest-exciton state in atomically smooth semiconductor quantum wires was first observed by Wegscheider *et al.*[6] in symmetric, T-shaped quantum wires made on the intersection of two 70-Å GaAs quantum wells surrounded by $Al_xGa_{1-x}As$ with the Al fraction $x=0.35$. Recently the same group obtained excitonic lasing in a 60-Å /140-Å asymmetric quantum wire with a 7% Al filled stem well (see Fig. 2).[8] They reported an interesting observation of two-mode lasing in this structure. Under strong excitation they achieved simultaneous lasing from two levels in the quantum wire. There is a switching between those two lasing modes as the temperature or pumping rate is changed. A simple rate equation model[14] gives very good agreement with experimental data, that suggests that we have lasing from two different states in the quantum wire.

All calculations published to date which include the Coulomb interaction between the electron and hole have only examined the ground-state exciton. They have used either variational methods[11–13] or other approximations[9,10] and were performed only for symmetric wires and for very limited cases realized experimentally in the early days of T-shaped wire manufacturing. With the growing experimental realization of these structures as well as the interesting report of lasing phenomena there is a need for accurate two-body calculations, treating on an equal footing the single-particle potential and the Coulomb interaction, of both the ground and excited states in the structure.

Excited states seem to be very important for the operation of excitonic lasers.[8] Calculations of energies, oscillator strengths for radiative recombination (i.e, how the various states couple to photons) as well as the full wave functions for the whole spectra of interest would be very beneficial for understanding the origins of certain transitions and effects. This could help in the design of lasers with better properties and higher maximum temperatures for excitonic lasing. The goal is to design excitonic lasers that can operate at room temperature. Also, performing highly accurate calculations of the ground-state exciton in QWR and the corresponding QW enables E_b and E_{con} to be obtained for different geometries (both symmetric and asymmetric) for a wide range of well widths and Al content, *x*. Such data are of great importance for the optimization of the structures.

Our method is based on an exact-numerical solution of the Schrödinger equation in a certain basis within the effective-mass approximation. The method is not restricted to a given number of excited states and we can calculate as many of them as required. For some structures we have calculated up to 100 excited states. We perform calculations for a very wide range of T-shaped wires. In Sec. II of the paper the numerical method is discussed in detail while in Sec. III we present the results. There we first study the spectra and wave functions and present a discussion of the nature of the various excited states. Finally we discuss E_{con}, E_b, and the difference between the ground-state exciton energy and the first excited-state energy E_{2-1} as a function of well width *Dx* and Al molar fraction *x* for the symmetric and asymmetric quantum wires.

II. THE MODEL

We use the effective-mass approximation with an anisotropic hole mass to describe an electron in a conduction band and a hole in a valence band in the semiconductor structures under consideration. The effective mass of the hole depends on the crystallographic direction in the plane of the T-shaped structure. We consider the heavy hole only. The other bands (split-off bands, light holes) would have energies higher than the region of interest for us. The light-hole exciton, the closest in energy to the heavy-hole exciton, is calculated to be over 30 meV higher that the heavy-hole exciton, and thus it is ignored in the calculations. The electron and hole are in the external potential of the quantum wire formed at the T-shaped intersection of the GaAs/$Al_xGa_{1-x}As$ quantum wells. The so-called arm quantum well is grown in the 110 crystal direction and intersects with a stem quantum well grown in the 001 direction (see Figs. 1 and 2). In our model the crystal directions 110, 001, and 110 correspond to *x*, *y*, and *z*, respectively. We consider symmetric quantum wires where the arm and stem well are both of the same width, i.e, $Dx=Dy$, and are made of GaAs. We also consider asymmetric wires where the stem well is significantly wider but filled with $Al_xGa_{1-x}As$ with a low Al content to compensate for the reduction in confinement energy. Our method is applicable to any structure regardless of its shape and materials provided the external potential is independent of *z*.

The value of the band gap is different for the different materials used in the well construction. This gives rise to the potential barriers at the interfaces between the GaAs, $Al_xGa_{1-x}As$ and $In_xGa_{1-x}As$ that take different values for electrons and holes. In our model the electron and hole are placed in external potentials $V_e(x,y)$ and $V_h(x,y)$, respectively, and interact via the Coulomb interaction. We choose the potential in GaAs to be zero and calculate all potentials in other materials with respect to this level. The external potential is independent of *z* in all cases. Sample geometries considered in this work are shown in Figs. 1 and 2. Using the above model, after the separation of the center of mass and relative motion in the *z* direction, the system is described by the following Hamiltonian:

$$H=-\frac{\hbar^2}{2m_e}\nabla^2_{x_e,y_e}-\frac{\hbar^2}{2m_{hx}}\nabla^2_{x_h}-\frac{\hbar^2}{2m_{hy}}\nabla^2_{y_h}-\frac{\hbar^2}{2\mu_z}\nabla^2_z + V_e(x_e,y_e)+V_h(x_h,y_h) - \frac{e^2}{4\pi\epsilon_0\epsilon\sqrt{(x_e-x_h)^2+(y_e-y_h)^2+z^2}}, \quad (2.1)$$

where $z=z_e-z_h$ and $1/\mu_z=1/m_e+1/m_{hz}$. The wave function associated with the center-of-mass motion in the *z* direction is a plane wave and this coordinate can be omitted from the problem.

A. Numerical method for calculating quantum-wire exciton states

We calculate the ground and excited states in the structures of interest by a direct-diagonalization method. Due to the complexity of the external potential with its limited symmetry and sharp edges, none of the standard basis sets seem appropriate. We use the following basis set:

$$\psi(x_e,y_e,x_h,y_h,z_e-z_h) = \sum_{i,j,k} c_{i,j,k}\sin\left(z\frac{k\pi}{L_z}-\frac{k\pi}{2}\right)\chi^e_i(x_e,y_e)\chi^h_j(x_h,y_h), \quad (2.2)$$

where $\chi^e_i(x_e,y_e)/\chi^h_j(x_h,y_h)$ are electron/hole single-particle wave functions for a T-shaped potential without the electron-hole Coulomb interaction. In the *z* direction we introduce hard-wall boundary conditions and use a standing-wave basis set.

Our basis set does not obey the so-called cusp condition[15] that is satisfied whenever two particles come together. The divergence in the potential energy when the electron and hole come together must be exactly canceled by an opposite divergence in the kinetic energy. The exact wave function must therefore have a cusp when the electron and hole are coincident. Using a basis in which every basis function obeys the cusp condition would reduce the size of the basis set required. For an isotropic hole mass it would be very easy to satisfy the cusp condition by multiplying the basis functions by the factor $\exp[-\Lambda\sqrt{(x_e-x_h)^2+(y_e-y_h)^2+z^2}]$ that is just the hydrogenic wave function. Unfortunately there is no analytical solution when we introduce the anisotropic hole mass. Thus we choose not to satisfy the cusp condition and therefore have to use a larger basis set.

The diagonalization is performed using a NAG library routine. Convergence is usually achieved with a basis set containing 20 of each of the single-particle wave functions and 20 standing waves in the *z* direction. Thus $20\times20\times20=8000$ basis functions are needed that gives 20^6 matrix elements. Only one quarter of the total number needs to be calculated as interchanging k_1 and k_2 leaves the matrix element unchanged while interchanging i_1 and j_1 with i_2 and j_2 gives its complex conjugate. This still leaves a great many matrix elements to be calculated. Thus to make the calculations feasible the matrix elements need to be calculated very rapidly (see Sec. II C).

B. Computational method for calculating the single-particle wave functions

The one-particle (electron and hole) wave functions, $\chi^e_i(x_e,y_e)$ and $\chi^h_j(x_h,y_h)$ in a T-shaped external potential are calculated using the conjugate-gradient minimization technique with preconditioning of the steepest descent vector. A detailed explanation of this method can be found in reference.[16] We specify the external potential on a 2D grid and use periodic boundary conditions in the *x* and *y* directions so that we are able to use fast Fourier transform (FFT) methods to calculate the kinetic energy in Fourier space while the potential energy-matrix elements are calculated in real space. The fast calculation of the energy-matrix elements is crucial as they have to be calculated many times during the conjugate-gradient minimization. The FFT provides very fast switching between real and Fourier space and

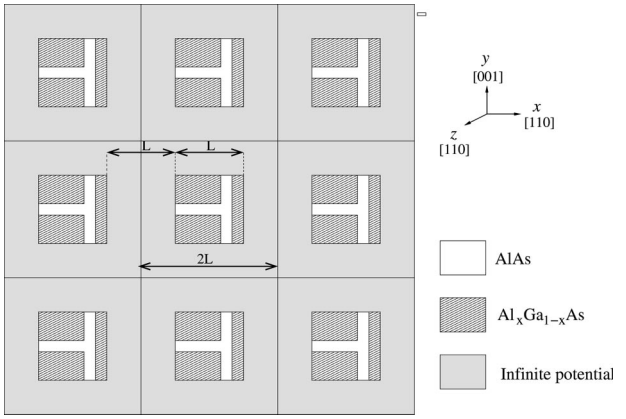

FIG. 3. Lattice used for calculations and notations.

makes the algorithm much more efficient, but the use of periodic boundary conditions introduces the problem of intercell interactions in the case of two-particle calculations. To avoid this problem we place the unit cell in the middle of another, larger unit cell of infinite potential (see Fig. 3 and the Sec. II C).

We use plane waves as a basis set for the one-particle problem. Using this method we can calculate as many as 50 states for the electron and 50 for the hole. Very good convergence with respect to the number of plane waves and the size of the unit cell is obtained (see Sec. III C).

C. Computational method for calculating the matrix elements

The kinetic and potential energies are diagonal in this basis and are obtained from the one-particle calculations. Thus only the Coulomb matrix elements need to be calculated.

A Coulomb matrix element in the basis set (2.2) is a 5D integral of the following form:

$$-\int\int\int\int\int dx_e\,dy_e\,dx_h\,dy_h\,dz \times\sin\left(z\frac{k_2\pi}{L_z}-\frac{k_2\pi}{2}\right)\chi^{e*}_{i_2}(x_e,y_e)\chi^{h*}_{j_2}(x_h,y_h)\, q(x_e-x_h,y_e-y_h,z) \times\sin\left(z\frac{k_1\pi}{L_z}-\frac{k_1\pi}{2}\right)\chi^{e}_{i_1}(x_e,y_e)\chi^{h}_{j_1}(x_h,y_h), \quad (2.3)$$

where $q(x_e-x_h,y_e-y_h,z)$ is the Coulomb interaction cut off at final distance to avoid image effects (see below). This integral must be calculated numerically. Numerical integration for so many dimensions is very slow and thus is not feasible for the case of 20^6 matrix elements. Thus another method has to be introduced.

The above integral is of the form

$$-\int\int\int\int\int dx_e\,dy_e\,dx_h\,dy_h\,dz\, f_e(x_e,y_e) \times f_h(x_h,y_h)q(x_e-x_h,y_e-y_h,z)f_z(z), \quad (2.4)$$

where

$$f_e(x_e,y_e)=\chi^{e*}_{i_2}(x_e,y_e)\chi^{e}_{i_1}(x_e,y_e),$$

$$f_h(x_h,y_h)=\chi^{h*}_{i_2}(x_h,y_h)\chi^{h}_{i_1}(x_h,y_h). \quad (2.5)$$

Using the Fourier transform and the convolution theorem it can be shown that the above integral is equal to

$$\int dz \sum_{G_x,G_y} F_e(-G_x,-G_y)F_h(G_x,G_y)Q(G_x,G_y,z), \quad (2.6)$$

where F_e, F_h, Q are the 2D Fourier transforms of the function f_e with respect to x_e and y_e, f_h with respect to x_h and y_h and q with respect to x_e-x_h and y_e-y_h, respectively. Thus the 5D integral can be reduced to a 1D integral with respect to the z variable and a 2D sum in Fourier space. The F_e and F_h Fourier transforms can be easily calculated using FFT's in real space after multiplication of the corresponding $\chi^{e}_{i_1}(x_e,y_e)$ by $\chi^{e*}_{i_2}(x_e,y_e)$ for electrons and $\chi^{h}_{i_1}(x_h,y_h)$ by $\chi^{h*}_{i_2}(x_h,y_h)$.

In order to use FFT's we need to introduce periodic boundary conditions in the x and y directions as in the one-particle calculations. To eliminate interactions between particles in neighboring cells, we place the unit cell in the middle of another, bigger unit cell of infinite potential (see Fig. 3).

The distance between the edges of successive small unit cells is exactly the width of the small unit cell, L. We cut off the Coulomb interaction at a distance corresponding to the size of the small unit cell. We therefore consider the following form of Coulomb interaction:

$$q(x_e-x_h,y_e-y_h,z)=\begin{cases} -\dfrac{e^2}{4\pi\epsilon_0\epsilon\sqrt{(x_e-x_h)^2+(y_e-y_h)^2+z^2}} & \text{if } x_e-x_h<L_x \text{ and } y_e-y_h<L_y \\ 0 & \text{otherwise.} \end{cases} \quad (2.7)$$

Particles interact only when their separations in the x and y directions are smaller than L_x and L_y, respectively. The separations of particles in neighboring cells is always bigger than the cutoff and thus they do not interact. Particles in the same unit cell are always separated by less than that the cutoff distance due to the infinite potential outside the small unit cell. Thus we take into account all of the physical Coulomb interaction and completely eliminate the interactions between images. In the numerical implementation the infinite potential is replaced by a large but finite potential. Thus the probability of the particle being outside the small unit cell is effectively zero and we find that the results do not depend on the value of this potential for values greater than around three times the potential in the $Al_xGa_{1-x}As$ region.

The 2D Fourier transform of the 3D Coulomb interaction with a cutoff cannot be done analytically. Thus we put the Coulomb interaction onto a 2D grid as a function of relative coordinates x_e-x_h and y_e-y_h for every z value. The unit cell in relative coordinates will go from $-L_x$ to L_x, and $-L_y$ to L_y, respectively. Then for every value of z a 2D FFT is performed with respect to x_e-x_h and y_e-y_h and the results stored in the 3D array $Q(G_x,G_y,z)$. Since this is the same for every matrix element the above calculation needs to be performed only once.

The calculations described by Eq. (2.6) need to be performed for every matrix element. After $F_e(G_x,G_y)$ and $F_h(G_x,G_y)$ have been calculated the summation over the reciprocal lattice vectors G_x and G_y for every value of z is performed. The remaining 1D integral in the z direction is done numerically, after interpolation of data points, using a routine from the NAG library. The dependence of the integrand on z is found to be very smooth and thus not many points are required to obtain accurate results.

III. RESULTS

We perform the calculations for a series of T-shaped structures. We calculate energies, oscillator strengths, and wave functions for the first 20–100 two-particle states for symmetric and asymmetric wires.

For symmetric wires we consider the structure denoted by W that has been experimentally studied by Wegscheider *et al.*[6] and consists of $GaAs/Al_{0.35}Ga_{0.65}As$ 70-Å quantum wells. Then, keeping the rest of parameters constant, we vary the quantum-well width from 10 Å to 80 Å in steps of 10 Å in order to examine the width dependence of the various properties. We also perform calculations for samples denoted by $S1$ and $S2$ studied by Someya *et al.*[3] made of $GaAs/Al_{0.3}Ga_{0.7}As$ ($S1$) and GaAs/AlAs ($S2$) quantum wells of width around 50 Å. For the GaAs/AlAs case we again vary the well width from 10 Å to 60 Å. Then we take an intermediate value of the Al molar fraction, $x=0.56$, and vary the well width from 10 Å to 60 Å in order to examine the dependence on the well width as well as Al content. Finally we perform calculations for 35-Å-scale $In_{0.17}Ga_{0.83}As/Al_{0.3}Ga_{0.7}As$ (denoted by $N4$) as well as for 40-Å-scale $In_{0.09}Ga_{0.91}As/Al_{0.3}Ga_{0.7}As$ (denoted by $N2$) samples as studied experimentally by Akiyama *et al.*[2]

For asymmetric structures we consider the wire studied experimentally by Rubio *et al.*[8] that consists of a 60-Å $GaAs/Al_{0.35}Ga_{0.65}As$ arm quantum well and a 140-Å $Al_{0.07}Ga_{0.93}As/Al_{0.35}Ga_{0.65}As$ stem quantum well. We vary the width of the arm quantum well from 50 Å to 100 Å. We also perform calculations for the asymmetric structure studied by a different group[4,5] that consists of a 25-Å $GaAs/Al_{0.3}Ga_{0.7}As$ arm quantum well and a 120-Å $Al_{0.14}Ga_{0.86}As/Al_{0.3}Ga_{0.7}As$ stem quantum well.

In the first part of this section we present the spectra for symmetric and asymmetric quantum wires with the positions of 2D exciton, 1D continuum (unbound electron and hole both in the wire) and 1De/2Dh continuum (unbound electron in the wire and hole in the well) states as well as pictures of representative wave functions. This allows us to discuss the nature of the excited states in the structures. In the second part we discuss the trends in confinement and binding energy and the separation in energy between the ground and the first-excited states as a function of the well width and Al fraction.

We use a static dielectric constant $\epsilon=13.2$ and a conduction-band offset ratio $Q_c=\Delta E_{cond}/\Delta E_g$ of 0.65. For the difference in band gaps on the $GaAs/Al_xGa_{1-x}As$ interface we use the following formula: $\Delta E_g=1247\times x$ meV for $x<0.45$ and $1247\times x+1147\times(x-0.45)^2$ meV for $x>0.45$. For the electron mass we use $m_e=0.067m_0$ while for the hole mass $m_{hx}=m_{hz}=m_{h[110]}=0.69-0.71m_0$ and $m_{hy}=m_{h[001]}=0.38m_0$ (m_0 is the electron rest mass). For the $In_{0.09}Ga_{0.91}As/Al_{0.3}Ga_{0.7}As$ ($In_{0.17}Ga_{0.83}As/Al_{0.3}Ga_{0.7}As$) we use parameters from Ref. 2: for the electron $m_e=0.0647(0.0626)m_0$, for the hole $m_{hy}=m_{hh[001]}=0.367(0.358)m_0$ and $m_{hx}=m_{hz}=m_{h[110]}=0.682(0.656)m_0$, $\Delta E_g=464(557)$ meV and the band offset was assumed to be 65% in the conduction and 35% in the valence band.

A. Excited states

1. Symmetric wires

In Fig. 4 we show spectra (the oscillator strength versus energy) for the first 20 (30 in the case of the 70-Å and 30-Å wire) states for the $GaAs/Al_{0.35}Ga_{0.65}As$ structure for well widths from 10 Å to 80 Å. A dashed line shows the energy of the 1D continuum, a dotted line that of the 1D electron and 2D hole continuum, the dotted-dashed line—the quantum-well 2D exciton, while the dashed-dot-dotted line shows the 2D electron and 2D hole continuum. In the case of the 20-Å wire the 2D electron and 2D hole continuum is not shown as its value of 245.5 meV is out of range by a significant amount. Because our system is finite in the z direction, we obtain only a sampling of the continuum states; below the continuum edge the states are discrete.

Note that for the experimentally studied 70-Å structure, the 2D exciton has a lower energy than the completely unbound electron and hole in the wire. The situation clearly depends on the well width and the crossing point is between 60 and 70 Å. For well widths of 60 Å or smaller, the 1D continuum (1Dcon) is lower in energy that the 2D exciton (2Dexc) with the difference being maximal for a width of around 20 Å. For widths of 70 Å or bigger, the 1Dcon is

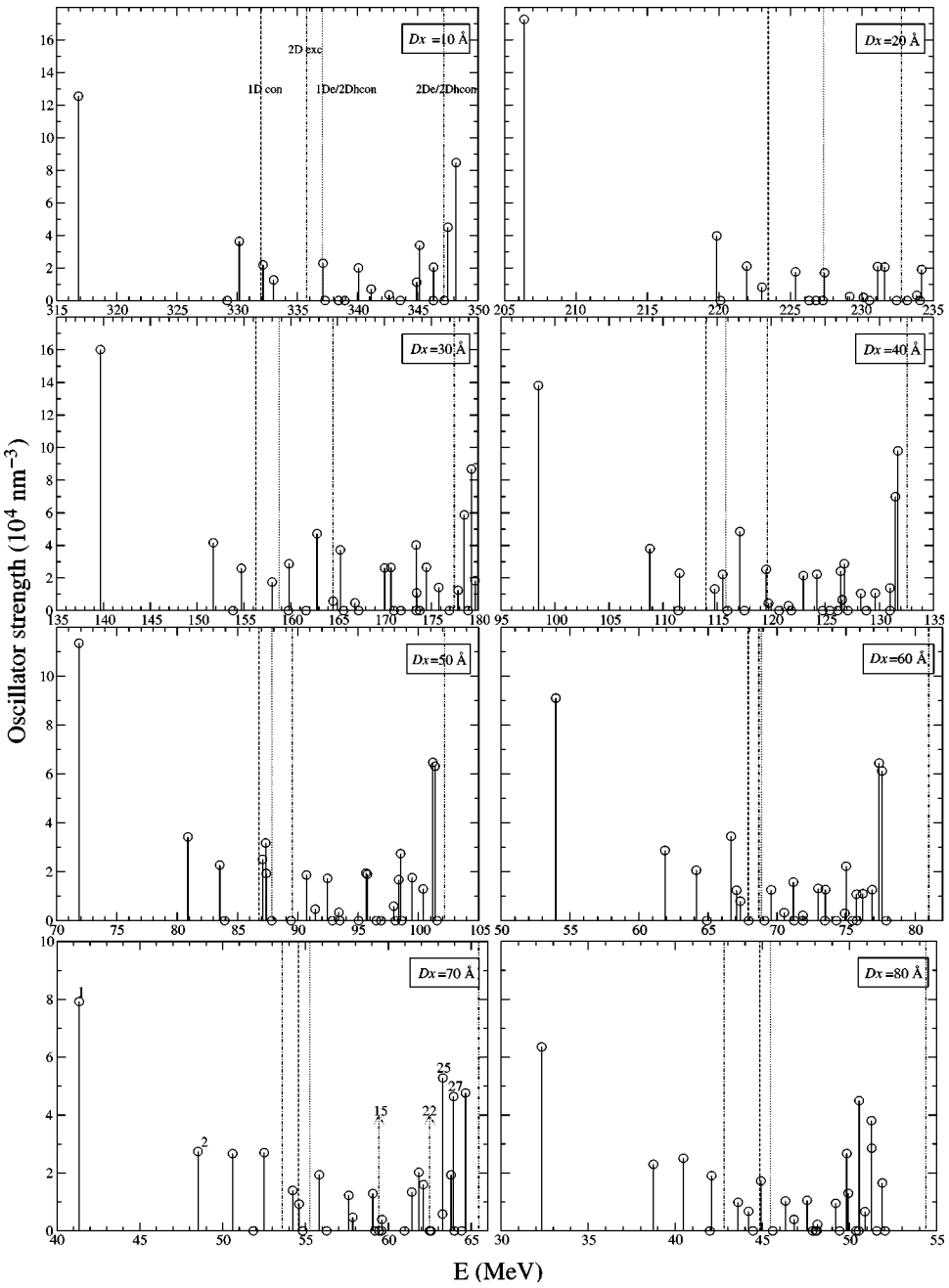

FIG. 4. Oscillator strength versus energy for the lowest 20–30 states in a symmetric T-shaped structure for different well widths Dx.

higher in energy than the 2Dexc with the difference growing for increasing well width. This effect might be significant for pumping T-shaped-wire lasers. Free electrons and holes are excited in the whole area of both wells and thus, when the 2D exciton has a lower energy than the 1D continuum, formation of the 2D excitons is energetically favourable. These excitons can recombine in a well instead of going to the wire and forming a 1D exciton. Clearly it is more efficient to have the 1D continuum lower in energy than the 2D exciton.

By increasing the well width we obtain more states that are lower in energy than the 1Dcon and 2Dexc beginning with two (ground and the first excited) for the 10-Å well, three for widths between 20–50 Å and four states for larger widths.

We now discuss the behavior of $|\psi|^2$ for the 70-Å case. The wave functions depend on five spatial coordinates and thus various cuts in 5D space are presented in Figs. 5 and 6: (a) the electron x_e, y_e position after averaging over the hole position, (b) the hole x_h, y_h position after averaging over the electron position, and relative coordinates after averaging over the center of mass position, (c) the x_e-x_h, y_e-y_h relative coordinates for $z_e-z_h=0$, and (d) the x_e-x_h, z relative coordinates for $y_e-y_h=0$.

For the ground state we observe that the electron and hole are very well localized in the wire with slightly more hole localization. The relative coordinate plots clearly show the bound exciton (Fig. 5 state 1).

The electron in the first-excited state is localized in the wire while the hole already expands into the arm well. The relative coordinate pictures show that the electron and hole are bound and form an exciton with an asymmetric shape. The size of the exciton is smallest in the x direction (the

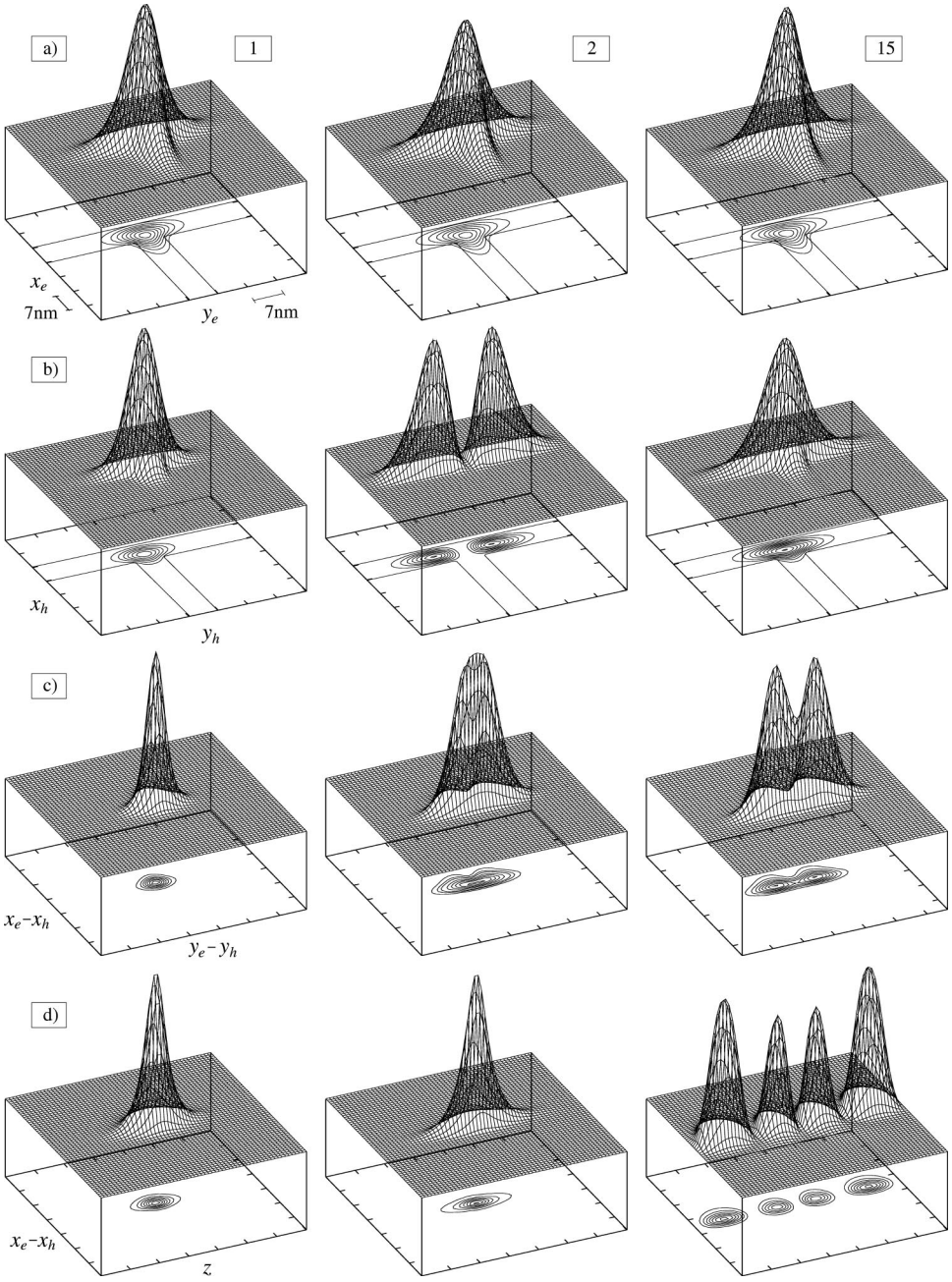

FIG. 5. Modulus squared of the two-particle wave function for the ground (1), first excited (2) and the 15th (15) state in the symmetric T structure. Electron (a), hole (b), and the relative coordinates $x_e - x_h$, $y_e - y_h$ (c), $x_e - x_h$, z (d) probability densities are shown.

stem-well direction) and the exciton expands more into the y (the arm well where the hole is expanded) and free z directions (Fig. 5 state 2). The oscillator strength of this state is about one-third of that of the ground state and the state clearly takes the form of a 1D exciton with its center of mass in the T wire.

It can be seen from the spectra (Fig. 4) that there are four states (apart from the ground state) with energies smaller than 1Dcon and 2Dexc. The nature of the third and fifth states is very similar to the second one: the center of mass is in the wire and the electron is still well localized in the wire while the hole spreads into the wells (into both the arm and stem wells for the third state while only into the stem well for the fifth one). The relative coordinates show the complex, asymmetric shape of this excitonic state and the oscillator strength is again around one-third of the ground-state exciton.

The fourth state with almost zero oscillator strength corresponds to a 1D continuum. The electron and hole are both in the wire but the relative coordinate pictures show an unbound exciton. Within the first 30 states we have three states of that nature: the 4th, 7th, and 15th. The 15th state is shown in Fig. 5: the electron and hole are confined in the wire (a, b) and there are 3 nodes in the z direction and 1 node in the y direction. The other two states look similar and differ only in the number of nodes. The energy of the fourth state, which is the lowest 1Dcon state, turns out to be lower than the real 1Dcon obtained from our one-particle calculations. This is due to the finite-size effects. Our method is very well converged with respect to the cell size for the bound state and

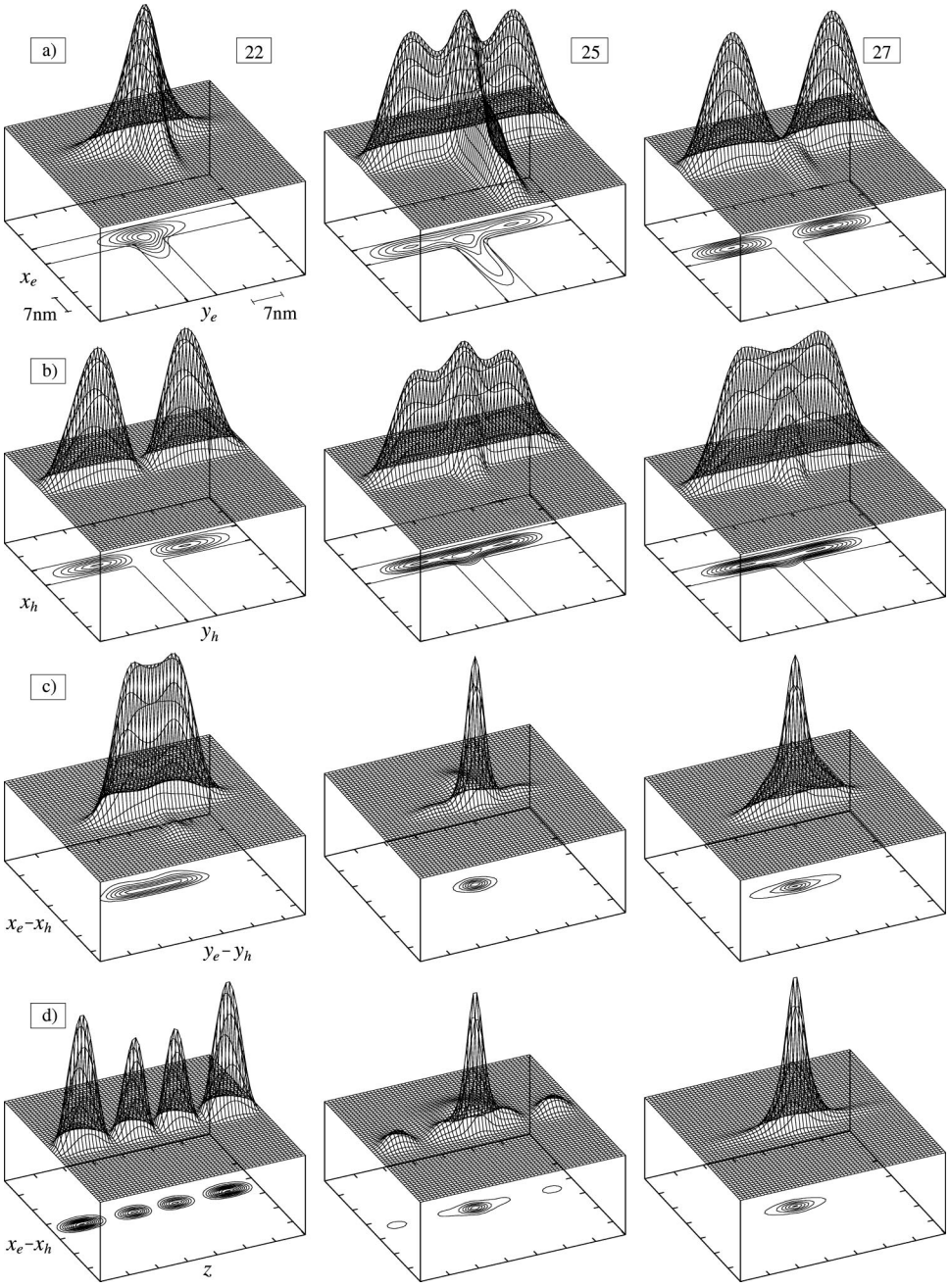

FIG. 6. Modulus squared of the two-particle wave function for the 22nd, 25th, and the 27th state in the symmetric T structure. Electron (a), hole (b), and the relative coordinates $x_e - x_h$, $y_e - y_h$ (c), $x_e - x_h$, z (d) probability densities are shown.

for the unbound ones where at least one of the particles is in the well. However, for the unbound continuum 1D states, the particles are very close in the x,y plane because of the very small size of the wire and thus the interaction is stronger. Consequently it does not decay as fast in the z direction as other states and thus we need a much bigger unit cell in the z direction to achieve convergence. There are however only three such states within the 30 we examine and we know their true energies from the preceding one-particle calculations.

For further excited states up to the 25th, the electron, and thus the center of mass, is still localized in the wire while the hole is taking up more and more energetic states in both wells, where energies are quantized due to the finite size of the cell. Those states can be divided into two groups depending on their relative coordinate nature: excitonic-like states similar to the second state (Fig. 5 state 2) and ionized states like the 22nd that is represented in Fig. 6 state 22. The oscillator strength of the second group is zero (see Fig. 4).

The 25th state (Fig. 6 state 25) is the first state where the electron is delocalized in both wells, the relative coordinates and the large oscillator strength shows that it is clearly an excitonic-like state. It appears to be a 2D quantum well exciton state scattered on the T-shaped intersection. Its energy is thus higher than that of a pure 2Dexc.

The 27th state is the 2D arm-quantum-well-exciton state. It has higher energy than the ground-state 2D exciton because the electron and hole wave functions occupy higher energy states than the ground state of the well due to the presence of the T intersection.

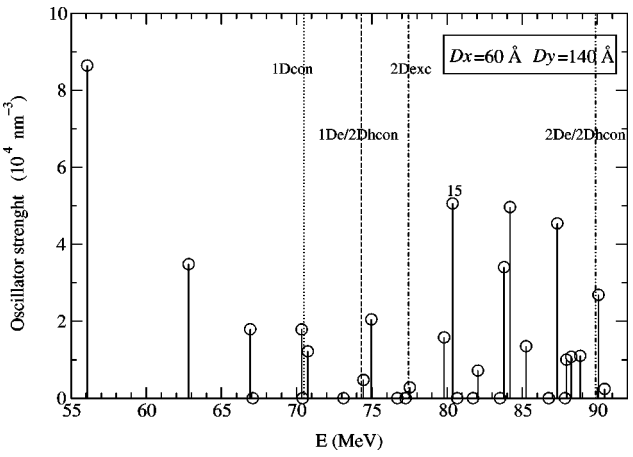

FIG. 7. Oscillator strength versus energy for the lowest 30 states in an asymmetric T-shaped structure with $Dx=60$ Å, $Dy=140$ Å.

The 30th state has a very similar nature as the 27th but the exciton expands into the stem instead of the arm quantum well.

The 25th, 27th, and 30th states all have large-oscillator strengths (around three-fourths of that of the ground-state exciton). It is interesting to note that between the ground state and those 2D large-oscillator-strength states, there is a group of states with relatively low-oscillator strengths. The reason for this is that after the ground state, there are states where either the wirelike electron is bound to the well-like hole and thus they do not overlap enough to give big contribution to the spectrum or they consist of a wirelike electron with an unbound hole.

Those quantum-well-like exciton states that scattered on the T-shaped potential (like state 25) appear to be quite important for the excitonic lasing because of their big oscillator strength. In Ref. 8 the authors reported two-mode lasing in an asymmetric wire where the laser switches between the ground-state exciton and the other state whose energy corresponds to the state from the tail of the above-mentioned states.

2. Asymmetric wires

The asymmetric wire that we study in detail consists of a 60-Å or 56-Å $GaAs/Al_{0.35}Ga_{0.65}As$ arm quantum well and a 140-Å $Al_{0.07}Ga_{0.93}As/Al_{0.35}Ga_{0.65}As$ stem quantum well.[8] The spectrum for the 60-Å arm case is shown in Fig. 7. The nature of the states is very similar to the case of the symmetric wire. The first two excited states are excitonlike and have an electron confined in the wire while the hole spreads into the well. All excited states up to the 20th have the electron confined in the wire. The hole spreads to one or both quantum wells taking up more energetic states in the well. The relative coordinates show either an excitonlike wave function (states with nonzero-oscillator strength in the spectra of Fig. 7) or the case where a hole is confined in the wire but is not bound to the electron (states with zero-oscillator strength in the spectra). Both groups were discussed and shown for the symmetric wire.

The 21st and the 24th states (large oscillator strengths in Fig. 7) have an electron expanding into the arm well. The electron wave function has a node in the wire region. The hole wave function spreads into the arm well and has no node for the 21st state and one node in the wire region for the 24th state. The relative coordinates show the excitonic nature of these states. Thus these states correspond to those 2D excitonic states scattered on the wire.

For the asymmetric structure we observe one state (the 15th, see Fig. 8) that does not correspond to any state in the symmetric case. The state is clearly excitoniclike with a large-oscillator strength and the relative coordinate plots show a very well bound exciton. The electron is confined in the wire in the same way as the ground state while the hole is clearly 1D-like, strongly confined in the wire but in a different way. It has a node in the wire region.

B. Trends in confinement and binding energies

1. Symmetric wires

We calculate the exciton binding energy, $E_b=E_e+E_h-E_{1Dexc}$, where E_e and E_h are the one-particle energies of an electron and a hole, respectively, in the wire. We also calculate, using the same method, the exciton energy in the quantum well, E_{2Dexc}, to obtain the confinement energy of the 1D exciton, $E_{con}=E_{2Dexc}-E_{1Dexc}$, in the wire.

We perform calculations for a wide range of structural parameters. For the $GaAs/Al_xGa_{1-x}As$ quantum wire we change the well width from 10 Å to 80 Å for three different values of the Al content x. The results are shown in Fig. 9. It can be noticed that for a well width bigger than 50 Å, changing the Al content has very little effect on the confinement and binding energies. The difference in binding energy between the 60-Å $GaAs/Al_{0.35}Ga_{0.65}As$ and the pure AlAs is only 1.5 meV. Thus it seems more promising to change the well width rather than the Al content for relatively wide wires. However, for thinner wires in the range of 10–50 Å, changing the Al content is much more profitable then changing the well width. The difference in binding energies for 20-Å wires with Al molar fractions of $x=0.3$ and $x=1.0$ is 6.4 meV. This increases to 10.6 meV when the width is reduced to 10 Å.

E_b and E_{con} for Al contents of $x=0.35$ and $x=0.56$ both approach a maximum for a well width between 10 Å and 20 Å. The maximum values for $x=0.35$ are $E_{bmax}=17.1$ meV, $E_{conmax}=26.4$ meV and for $x=0.56$ they are $E_{bmax}=19.7$ meV, $E_{conmax}=41.4$ meV. For the $x=1.0$ case, the curve does not have a maximum in the region for which calculations has been performed but we consider going to wells thinner than 10 Å as practically uninteresting. Thus the maximum energies are for $Dx=10$ Å and they are $E_{bmax}=25.8$ meV and $E_{conmax}=87.8$ meV.

E_{con} increases much more rapidly than E_b when the well width is progressively reduced. The curves cross for a well width between 60 Å and 70 Å, i.e. for widths of 60 Å or smaller, E_{con} is greater that E_b that means that the 1D continuum is lower in energy than the 2D exciton (as we discussed in Sec. III A 1) with the difference having a maximum at around 20 Å. For widths of 70 Å or bigger, E_b is

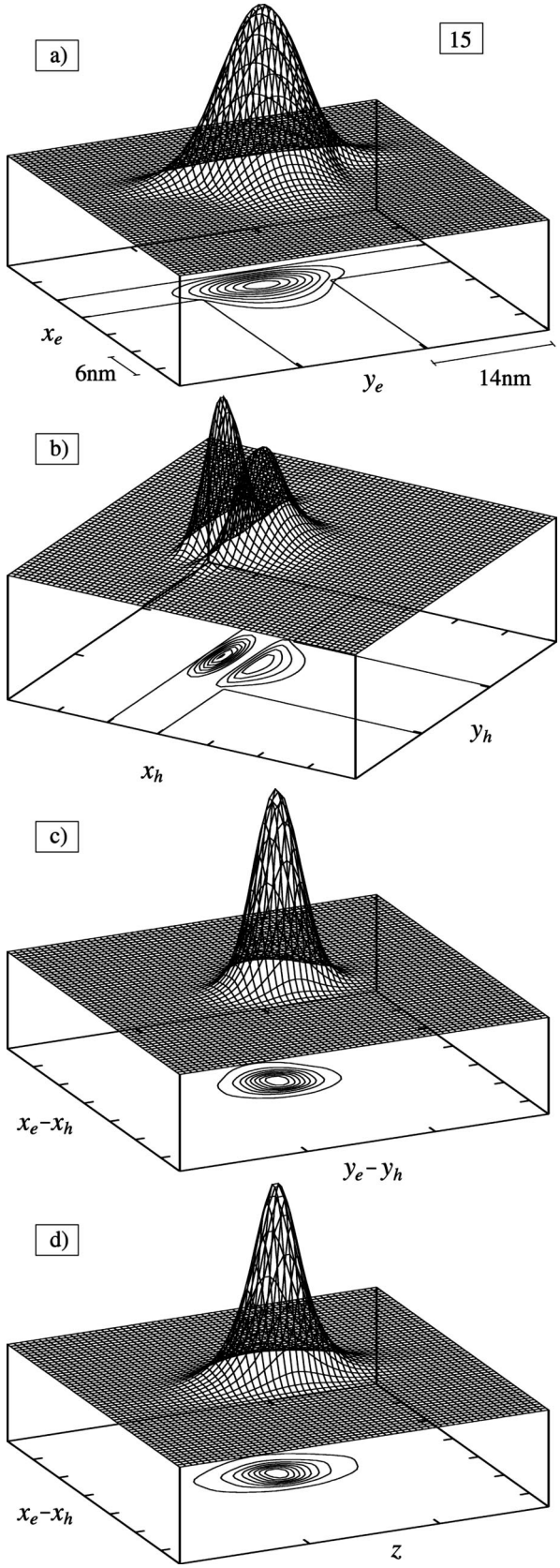

FIG. 8. Electron (a), hole (b), and the relative coordinates $x_e - x_h$, $y_e - y_h$ (c), $x_e - x_h$, z (d) probability densities for the 15th state in an asymmetric T-shaped structure with $Dx = 60$ Å, $Dy = 140$ Å.

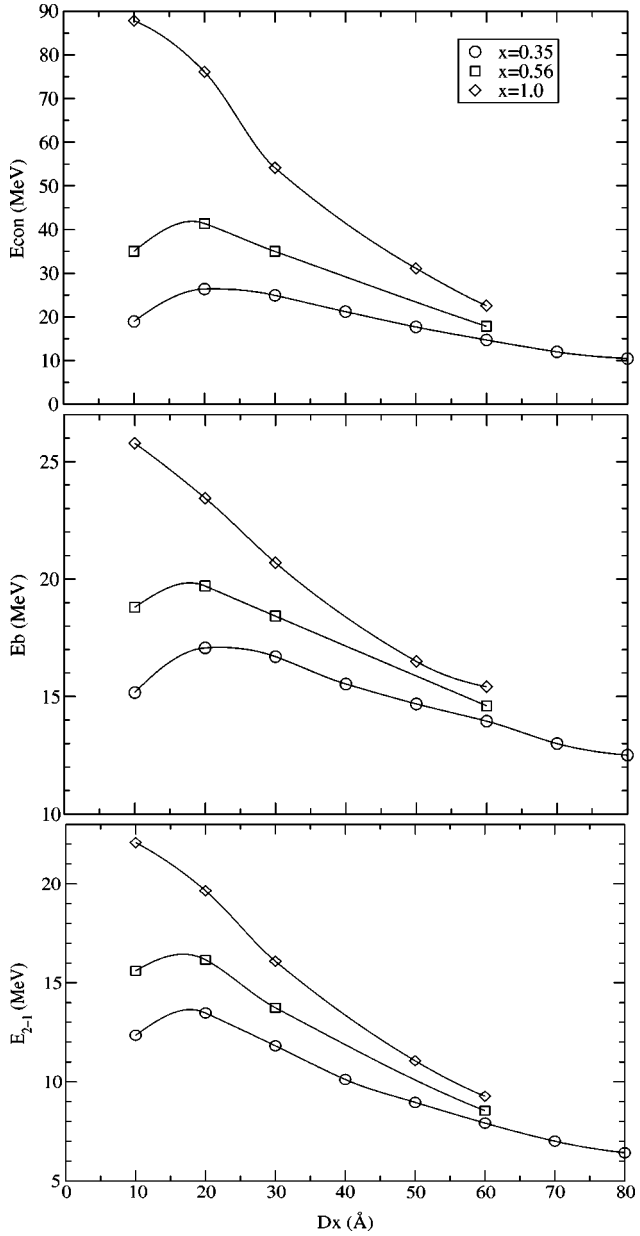

FIG. 9. Confinement energy $E_{con} = E_{2Dexc} - E_{1Dexc}$, binding energy of the ground-state exciton E_b, and the energy difference between the ground state and the first-excited state E_{2-1} as a function of the well width Dx in a symmetric T structure for three different aluminium molar fractions x.

greater than E_{con} with the difference growing for increasing well width. We also consider the difference in energy between the ground-state exciton in the wire and the first-excited state as a function of the well widths. For the experimentally realized $Dx = 70$-Å case, this difference is $E_{2-1} = 7.0$ meV and the maximum value for $Dx = 10$ Å is $E_{2-1max} = 13.5$ meV. The maximum value for the GaAs/AlAs at $Dx = 20$ Å is 22 meV.

Although pure AlAs gives the biggest potential offsets and thus the biggest binding and confinement energies, the GaAs/AlAs interfaces are not very smooth, which influences the transport properties. Thus new materials have to be pro-

TABLE I. Binding energy E_b and the confinement energy $E_{con}=E_{1Dexc}-E_{2Dexc}$ in meV of the QWR exciton for five different samples W, S_1, S_2, N_2, N_4 obtained from different methods.

	W [a]		S_1 [b]		S_2 [b]		N_2 [c]		N_4 [c]		R [d]		G [e]	
Method	E_b	E_{con}	E_b	E_{con}	E_b	E_{con}	E_b	E_{con}	E_b	E_{con}	E_b	E_{con}	E_b	E_{con}
Expt [f]	17	17	17	18	27	38		28		34	13.8	23		54
This work	13	12	14.3	17.8	16.5	31.1	12.1	26.3	16.5	31.2	13.5	21.4	14.6	36.4
Nonvar1 [g]	13.2		14.3		16.4									
Nonvar2 [h]			11.63		13.9									
Var1 [i]			15		18									
Var2 [j]	9.6	11.9												
Var3 [k]	12	14												

[a]Sample and experimental values from Ref. 6.
[b]Sample and experimental values from Ref. 3.
[c]Sample and experimental values from Ref. 2.
[d]Sample and experimental values from Ref. 8.
[e]Sample and experimental values from Refs. 4 and 5.
[f]E_{con} is obtained experimentally from the shift between QW and QWR exciton lines. The E_b is obtained indirectly from experimental measurement of the QWR exciton line and one-particle calculations.
[g]Results of calculations from Ref. 9.
[h]Results of calculations from Ref. 10.
[i]Results of variational calculations from Ref. 11.
[j]Results of variational calculations from Ref. 12.
[k]Results of variational calculations from Ref. 13.

posed. Two structures based on InGaAs have been manufactured and measured:[2] 35-Å-scale $In_{0.17}Ga_{0.83}As/Al_{0.3}Ga_{0.7}As$ ($N4$) and 40-Å-scale $In_{0.09}Ga_{0.91}As/Al_{0.3}Ga_{0.7}As$ ($N2$). The results of calculations for these structures are presented in Table I. It can be seen that energies for the sample $N4$ are almost exactly the same as for the GaAs/AlAs sample $S2$ suggesting that these materials might be very good candidates for structures with large-exciton confinement and binding energies.

2. Asymmetric wires

In order to increase binding and confinement energies, the asymmetric T-shaped structure was proposed and realized by two groups.[8,4,5]

We calculate E_b and E_{con} for the 60-Å /140-Å structure with the stem quantum well filled with 7% Al in order to compare with experiment[8] and then we vary the width of the arm well from 50 to 100 Å. One can see from Fig. 10 that the binding energy is almost independent of the arm well width in this region, changing only from the maximum value of 13.5 meV for $Dx=60$ Å to 11.5 meV for $Dx=100$ Å. The binding energy for the 60-Å symmetric wire with the same $x=0.35$ Al mole fraction is 13.9 meV—a bit bigger than for the asymmetric structure. In contrast, the confinement energy E_{con} changes rapidly with the width of the arm well from 4.7 meV for $Dx=100$ Å up to 33.3 meV for $Dx=50$ Å. For arm well widths of 60 Å or bigger, the 2D quantum-well exciton in the arm well has a lower energy than that for the stem well, thus the confinement energy is calculated with respect to the arm well exciton. For the 50-Å -wide arm well, the 2D exciton has higher energy than for the stem quantum well and thus the confinement energy is calculated with respect to the stem quantum well. Therefore 33.3 meV is the highest confinement energy for this stem well and changing the arm well would have no effect. Thus the 60-Å /140-Å structure is well optimized and its confinement energy E_{con} is 21.4 meV that is much bigger than that of 14.7 meV for the 60-Å symmetric wire.

The highest confinement energy so far reported is for an asymmetric $GaAs/Al_{0.35}Ga_{0.65}As$ wire with a 25-Å arm quantum well and a 120-Å stem quantum well filled with 14% Al.[4,5] The experimentally obtained E_{con} for this structure is 54 meV. Our calculations however give only 36.4 meV that is still the highest among experimentally obtained structures

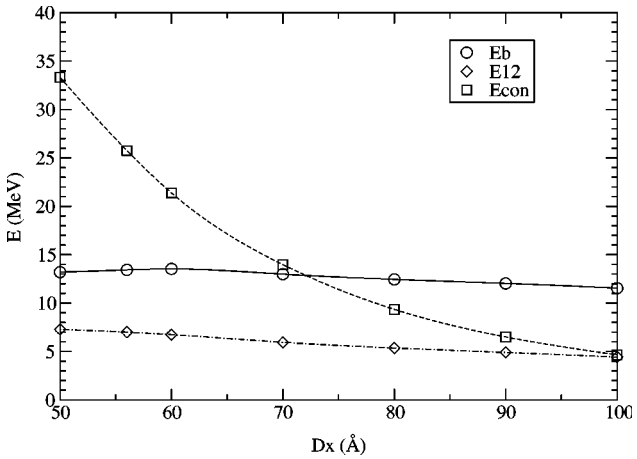

FIG. 10. Confinement energy $E_{con}=E_{2Dexc}-E_{1Dexc}$, binding energy of the ground-state exciton E_b, and the difference between the ground and the first-excited state E_{2-1} for an asymmetric wire as a function of the well width Dx, where $Dy=140$ Å.

but much lower than reported by the authors. Our calculation of E_{con} for five different experimentally realized structures agree very well with the experimental values and thus it is very probable that the value of 54 meV is overestimated. The binding energy from our calculations is only 14.6 meV for this structure.

We can conclude from our results that the optimized asymmetric structure does not lead to a bigger exciton binding energy than the symmetric ones with the same parameters. The confinement energy is considerably enhanced and this effect, which can be measured directly, has often been used to infer that the binding energy is increased. However, our results show that no such relationship holds between the confinement and binding energies. Thus the biggest confinement energy of any structure constructed so far of 36.4 meV does not lead to the biggest binding energy. Indeed, the binding energy of 14.6 meV is smaller than the 16.5 meV reported for the GaAs/AlAs 50-Å-scale symmetric structure[3] where the confinement energy should be only 31.1 meV. It is also smaller than expected for a symmetric 25-Å-scale structure with the same parameters (16.0–16.5 meV). Thus asymmetric structures could be useful for applications where a large confinement energy is required but appear to be less suitable than symmetric wires for applications where large binding energies are of interest.

3. Comparison with experiment and other calculations

The comparison between experiment and other published calculations is presented in Table I. The confinement energy of the exciton can be directly measured experimentally. Although, due to the strong-inhomogeneous broadening of the photoluminescence peaks, the accuracy of this number is not very high, it is the only experimentally proven quantity we can refer to. The experimental binding energy needs to be calculated using both experimental data and one-particle calculations and thus errors might accumulate. Other theoretical methods that we refer to obtain the ground-state exciton energy using variational techniques[11–13] (they differ in the form used for the variational wave functions). There are also two nonvariational calculations for the ground-state exciton.[9,10]

Our results for the confinement energy of the ground-state exciton E_{con} agree very well with experimental values for samples $S1$, $N2$, and $N4$ to an accuracy of 1%, 6%, and 8%, respectively. This is indeed very good agreement taking into account the strong-inhomogeneous broadening of the peaks they present. The spectral line width of the photoluminescence peaks according to the authors is around 15 meV that corresponds to a thickness fluctuation of about 3 Å for $N2$ and $N4$.[2] For the $S1$ and $S2$ samples the authors estimate the experimental error due to the inhomogeneous broadening as 2 meV. Agreement between our calculations and experiment is not as good for the $S2$ sample but for this case additional effects are present. For example, AlAs barriers give much less smooth interfaces than the lower Al fraction samples and this is not taken into account in our model. There is also very good agreement (better than 7%) between our results and the experimental measurement[8] for asymmetric wire R. The earlier E_{con} published by this group for the symmetric structure W is probably slightly overestimated.

All calculations published to date use the effective-mass approximation model for the heavy-hole exciton. Values of potential barriers used in the calculations vary depending on the publication. We have examined the influence of these differences on the final results (see Sec. III C). Both binding and confinement energies can differ by approximately 0.5 meV.

There are only two calculations published for the confinement energy. They are based on variational methods and were performed only for sample *W*. Variational method 2 (Ref. 12) uses a wave function that takes into account correlation in all spatial direction and the agreement with our results is very good for the confinement energy but not so good for the binding energy.

The variational method proposed by Kiselev and Rossler[13] and denoted here as method 3 has a trial wave function that has only *z* dependence in the correlation factor. Their binding energy for the sample *W* differs by only 1 meV from our result but their value for the confinement energy differs from ours. They perform calculations of the binding energy for the whole range of well widths Dx from 10–70 Å. This can be compared with our results in Fig. 9. Their calculations, like ours, give the maximum for E_b and E_{con} for a well width of around 20 Å. Their binding energy is a bit bigger than the one from our calculations. They obtained a maximum of $E_b = 18.6$ meV that is 1.5 meV higher than our result. However, their confinement energy $E_{conmax} = 33.0$ meV differs by 7 meV from our result. Their values of E_{con} are probably overestimated. They use the variational technique to calculate the quantum-wire exciton energy but the quantum-well exciton energy is taken from some other calculations of excitons in quantum wells performed using a different method and with different parameters, thus errors may accumulate.

The variational method 1,[11] which uses yet another form of trial wave function, has been applied to samples $S1$ and $S2$ to calculate the binding energy E_b. It agrees quite well with our and other accurate methods.

The binding energy we obtain shows excellent agreement with other nonvariational calculations by Glutsch *et al.*[9] (see Table I). They calculated the binding energy only for samples *W*, $S1$, and $S2$ and thus unfortunately the confinement energy cannot be compared. The method presented in Ref. 10 gives much lower values for the binding energy than all other methods.

Despite some small differences, all of the theoretical methods give much smaller values for E_b than the experimental estimates. One has to bear in mind, however, that the ''experimental'' values for E_b (quoted in the Table I) are in fact derived from a combination of experimental data and associated theoretical modeling, with inherent uncertainties. Our results come from direct diagonalization and are very well converged. Therefore we believe that the experimental binding energies are, in some cases, considerably overestimated. The real binding energy is thus smaller than has been claimed and the biggest value for any of the structures manufactured so far is 16.5 meV for samples $S2$ and $N4$.

C. Accuracy of the results

In our method the one-particle energies and wave functions are calculated first. The one-particle energies are very well converged with respect to all the variables such as unit cell size, number of points on the grid and the number of plane waves to an accuracy of 0.1 meV. We use on average as many as 160 000 plane waves that correspond to 400 $\times$400 points on the grid (200$\times$200 in the small unit cell). We obtain excellent agreement between our energies for the single electron and hole and those obtained by Glutsch *et al.*[9] For the 70 Å, $x=0.35$ symmetric quantum wire we obtain $E_e=47.09$ meV and $E_h=7.47$ meV while their results are $E_e=47.2$ meV and $E_h=7.5$ meV. According to our calculations there is only one electron state confined in the wire and its confinement energy E_{2D-1D} (i.e., the difference between well-like and wirelike-electron states) is 9 meV. This is in very good agreement with other methods. Pfeifer *et al.*[17] using 8 band $\vec{k}\cdot\vec{p}$ calculations obtained a confinement energy of 8.5 meV for the same structure. Kiselev and Rossler[13] using the so-called free-relaxation method obtained approximately the same value of 9 meV.

These one-particle wave functions are then used as a basis set for the two-particle calculations. The E_{1Dexc} is very well converged with respect to the number of points on the grid (as for the one-particle calculations), and with the size of the basis set. Convergence is usually achieved with about 20 $\times$20$\times$20 (8000) basis functions. In order to minimize finite-size effects we use quite big unit cells [from 43 times the well width, Dx for very thin wires (10 Å) to 7 times Dx for the 80 Å wire]. The exciton energy E_{1Dexc} is converged to within about 0.2 meV and E_{2Dexc} to within 0.3 meV that gives an accuracy for E_b of about 0.3 meV and for E_{con} of about 0.5 meV.

The other problem that can influence the accuracy of the results is the uncertainty associated with the input parameters. The electron and hole masses as well as the dielectric constant are standard but the potential barriers vary a lot depending on the publication. We have found quite different values of the potential offsets for the same material interfaces in the literature. We have examined the influence of this uncertainty on the final results by performing calculations for the extrema of the sets of parameters found. Both binding and confinement energies can differ by approximately 0.5 meV.

For the parameters that we are using, the results are converged to within 0.3 meV for the binding and 0.5 meV for the confinement energies. However, one needs to remember that these parameters are not well calibrated and this could lead to an additional error in both energies of about 0.5 meV.

The first few (4 in the case of Fig. 7) excited states of the wire that are below the 1Dcon and the 2Dexc are discrete, quasi-1D excitonic states and are converged to within 1 meV. Convergence of the higher states in the continuum is more complicated. Because our system is finite we obtain only a sampling of the continuum states. When we increase the unit-cell size we automatically calculate more states within the same energy region and they do not have a one-to-one correspondence with the states calculated using a smaller unit cell. The new states appear in between the old ones, with smaller oscillator strengths so that the total oscillator strength is conserved. When the Gaussian broadening of a 4 meV full width at half maximum is added to the spectra then for a sufficiently big unit cell the broadened spectrum is independent of the unit cell, thus convergence is reached. The spectra shown in Figs. 4 and 7 are converged in the sense that the continuum is accurately sampled on the scale of 4 meV.

IV. SUMMARY

We have performed an exact diagonalization within a finite-basis set of the Hamiltonian that describes an interacting electron-hole pair in a T-shaped quantum wire. We have obtained the ground- and excited-state energies and wave functions for this system. The first group of excited states shows an *s*-like excitonic character where the electron is localized in the wire but is bound to the hole that spreads into one of the wells. Due to the fact that the electron and hole are not localized in the same region, we have a group of low oscillator-strength states just above the ground state. This group is followed by a number of states with large-oscillator strength that are 2D excitonic states scattered on the T-shaped intersection. The excitonic lasing from one of those states has been experimentally observed.[8] We have also performed a detailed study of the exciton binding and confinement energies as a function of the well width and Al molar fraction for symmetric and asymmetric wires. The highest binding energy in any structure so far constructed is calculated to be 16.5 meV that is much smaller than previously thought. Our results have shown that for optimized asymmetric wires, the confinement energy is enhanced but the binding energy is slightly lower with respect to those in symmetric wires. For GaAs/Al_xGa_{1-x}As wires we have obtained an upper limit for the binding energy of around 25 meV in a 10-Å -wide GaAs/AlAs structure that suggests that other materials need to be explored in order to achieve room-temperature applications. $In_yGa_{1-y}As/Al_xGa_{1-x}As$ might be a good candidate.

ACKNOWLEDGMENTS

We are pleased to thank P. Haynes, G. Rajagopal, A. Porter, Y. Mao, and G. McMullan for very beneficial discussions concerning the computational techniques and L. N. Pfeiffer, A. Pinczuk, J. Rubio, and H. Akiyama for stimulating discussions and communicating experimental results prior to publication. M.H.S acknowledges financial support from Lucent Technologies, Trinity College Cambridge and an ORS award.

[1] Y. C. Chang, L. L. Chang, and L. Esaki, Appl. Phys. Lett. **47**, 1324 (1985).
[2] H. Akiyama, T. Someya, M. Yoshita, T. Sasaki, H. Sakaki, Phys. Rev. B **57**, 3765 (1998).
[3] T. Someya, H. Akiyama, and H. Sakaki, Phys. Rev. Lett. **76**, 2965 (1996).
[4] H. Gislason, W. Langbein, and J. M. Hvam, Superlattices Microstruct. **22**, 217 (1997).
[5] W. Langbein, H. Gislason, and J. M. Hvam, Phys. Rev. B **54**, 14 595 (1996).
[6] W. Wegscheider, L. N. Pfeiffer, M. M. Dignam, A. Pinczuk, K. W. West, S. L. McCall, and R. Hull, Phys. Rev. Lett. **71**, 4071 (1993).
[7] J. Hasen, L. N. Pfeiffer, A. Pinczuk, S. He, K. W. West, and Brian S. Dennis, Nature (London) **390**, 54 (1997).
[8] J. Rubio, L. N. Pfeiffer, M. H. Szymanska, A. Pinczuk, S. He, H. U. Baranger, K. W. West, B. S. Dennis, and P. B. Littlewood (unpublished).
[9] S. Glutsch, F. Bechstedt, W. Wegscheider, and G. Schedelbeck, Phys. Rev. B **56**, 4108 (1997).
[10] F. Rossi, G. Goldoni, and E. Molinari, Phys. Rev. Lett. **78**, 3527 (1997).
[11] D. Brinkman and G. Fishman, Phys. Rev. B **56**, 15 211 (1997).
[12] G. W. Bryant, P. S. Julienne, and Y. B. Band, Superlattices Microstruct. **20**, 601 (1996).
[13] A. A. Kiselev and U. Rossler, Semicond. Sci. Technol. **11**, 203 (1996).
[14] J. Rubio, L. N. Pfeiffer, M. H. Szymanska, A. Pinczuk, S. He, H. U. Baranger, K. W. West, B. S. Dennis, and P. B. Littlewood (unpublished).
[15] T. Kato, Commun. Pure Appl. Math. **10**, 151 (1957).
[16] M. C. Payne, M. P. Teter, D. C. Allan, T. A. Arias, and J. D. Joannopoulos, Rev. Mod. Phys. **64**, 1045 (1992).
[17] L. Pfeifer, H. Baranger, D. Gershoni, K. Smith, and W Wegscheider, in *Low Dimensional Structures Prepared by Epitaxial Growth or Regrowth on Patterned Substrates*, edited by K. Eberl *et al.* (Kluwer Academic, 1995), pp. 93–100.